Int. J. Electrochem. Sci., 17 **(2022)** Article Number: 22114, doi: 10.20964/2022.11.23

International Journal of
ELECTROCHEMICAL
SCIENCE
www.electrochemsci.org

Comparison of Electrocatalytic Hydrogen Evolution Properties of Ni-Co and Ni-Co-WC Porous Electrodes

Yufang Yang

School of Material Science and Engineering, Hanshan Normal University, Chaozhou 521041, China
E-mail: zzyufang@163.com

Received: 3 June 2022 / *Accepted:* 2 September 2022 / *Published:* 10 October 2022

The porous electrode of $(Ni\text{-}Co)_0$ and $(Ni\text{-}Co)_{30}$ for electrocatalytic hydrogen evolution were prepared by electroplating on a sponge Co based alloy $Co_{69.9}Ni_{30.1}$ matrix. Scanning electron microscope (SEM) and X-ray diffractometer (XRD) were used to characterize the surface images and the crystal structure of the electrodes, respectively. Polarization curves, electrochemical reaction AC impedance spectroscopy (EIS), cyclic voltammetry (CV) curves and amperometric i-t curves were used to compare their electrocatalysis for hydrogen evolution reaction (HER) in the dilute sulphuric acid solution with concentration of 0.5M. The surface of the composite coating $(Ni\text{-}Co)_{30}$ is densely packed with coarse particles like peanut shell, which are agglomerated by a large number of tiny particles. The specific surface ratio of $(Ni\text{-}Co)_{30}$ is higher than that of the $(Ni\text{-}Co)_0$ coating. The structure of $(Ni\text{-}Co)_{30}$ is a biphasic structure with WC dispersed in the Ni-Co solid solution. The results show that the HER overpotential, the electrochemical impedance and the apparent activating energy of the reaction of hydrogen evolution for the porous $(Ni\text{-}Co)_{30}$ are lower than those of the porous $(Ni\text{-}Co)_0$. When the temperature is 25-50℃, the exchange current density of HER for $(Ni\text{-}Co)_{30}$ is 8.92-15.78 times greater than that of the porous $(Ni\text{-}Co)_0$. The HER overpotential of $(Ni\text{-}Co)_{30}$ at a current density of $10mA/cm^2$ is 0.118V lower than that of $(Ni\text{-}Co)_0$. The activation energy of the HER of the $(Ni\text{-}Co)_{30}$ at the overpotential of 0.2V is 20kJ/mol smaller than that of the $(Ni\text{-}Co)_0$. The $(Ni\text{-}Co)_{30}$ has excellent oxidation resistance and super HER stability, as does the $(Ni\text{-}Co)_0$. The electrocatalytic HER performance of the composite electrode $(Ni\text{-}Co)_{30}$ is better than that of the $(Ni\text{-}Co)_0$.

Keywords: Comparison; Electrocatalysis; Hydrogen evolution reaction; Ni-Co; Ni-Co-WC; Composite; Porous electrode;

1. INTRODUCTION

Hydrogen is a clean energy carrier with low mass density and high energy density, which is expected to replace fossil fuels and can be recycled continuously. Therefore, it is regarded as the most ideal clean energy [1-5]. There are many methods to prepare hydrogen, such as fossil fuel cracking, methane steam reforming, the water gas method, water electrolysis method and photoelectrochemical

water splitting method, etc. Among them, the electrocatalytic hydrogen evolution reaction (HER) of water, due to its advantages of amity environment, is an important means to generate hydrogen cheaply in industry. However, electrocatalytic HER provides about 5% hydrogen in the global market, and the rest is mainly produced by catalytic steam reforming of natural gas [6,7]. This is mainly due to the lack of a durable and excellent electrocatalyst, which leads to the lower market share of electrocatalytic HER. Therefore, improving the activity of the electrocatalyst and reducing the overpotential of HER are the main ways to reduce energy consumption in electrocatalytic hydrogen production industry. However, the overpotential of electrocatalytic HER of most electrode materials is higher, resulting in large energy consumption of electrolysis. The development of electrodes with low cost, high electrocatalytic activity and low HER overpotential has become one of the key problems to be researched. The important methods to reduce the overpotential of HER are to increase the porosity, surface roughness and specific area of the cathode, or by selecting new HER materials with high catalytic activity to enhance the electrochemical activity of the electrode itself. According to the famous volcano plot, the maximum rate of HER occurs when the M-H bond strength is medium. The most active metals for HER are placed on top of the "volcano" curve [8]. The noble metals Pt, Rh and Ir are just located at the top of the volcanic curve, having a low HER overpotential and high electrocatalytic activity. However, due to being rare and expensive, Pt and Ir are not suitable for large-scale use in industrial production. The bond strength of the adsorbed hydrogen M-H of Ni is moderate, so Ni and nickel based materials show higher electrocatalytic HER activity. Moreover, nickel has the advantages of a low price and wide sources, which is favored by researchers. There are many reports on the electrocatalytic HER properties of nickel based multicomponent alloy materials, including binary materials Ni-S[9], Fe-Ni[10], Ni-Mo[11-17], Ni-Co[18-21], Ni-W[22], ternary material Ni-Co-Y[23], Ni-Co-Sn[24], Co-Ni-graphite[25], Ni-Co-Mo[26-27], quaternary material Co-Ni-Fe-C[28], etc. These electrodes are usually prepared on a bulk substrate. However, the porous electrode has a larger specific surface than the bulk electrode, which is more suitable for electrolytic HER[29-34]. Different porous substrate materials show significantly different electrocatalytic HER properties. In this paper, the porous electrodes of Ni-Co and Ni-Co-WC were prepared by electroplating on the three-dimensional foam Co-Ni alloy substrate. Their electrocatalytic HER properties were compared by cathodic polarization, AC impedance, cyclic voltammetry and chronoamperometry.

2. EXPERIMENTAL

2.1. Preparation of $(Ni\text{-}Co)_0$ and $(Ni\text{-}Co)_{30}$ porous electrode

The electrolytic nickel block was served as the anode, the sponge cobalt based alloy with 69.9wt.%Co and 30.1wt.%Ni ($Co_{69.9}Ni_{30.1}$) was used as the cathode. The porosity of the matrix is 98%, the pore diameter is 200um and its thickness is 1mm. The cathode area to be plated is $5cm^2$, the area ratio of cathode to anode is 1:2.5.

Before electroplating, the foam $Co_{69.9}Ni_{30.1}$ substrate was degreased in 80℃ alkaline degreasing solution with the KQ-50B ultrasonic washing device, cleaned and dried in oven. The plating solution

was composed of 0.52M H_3BO_3 ,0.2M $NiCl_2 \cdot 6H_2O$, 0.46M $NiSO_4 \cdot 6H_2O$, 0.08M $CoSO_4 \cdot 7H_2O$, 30g/L WC and 0.1g/L wetting agent. All reagents are analytically pure and dissolved in deionized water. The WC powder with an average particle size of 200 mesh was added to the electroplating solution and thoroughly agitated by a stirrer, so as to completely disperse the WC powder in the plating solution. The electroplating was carried out at a current density of 4A/dm^2, a temperature of 40℃ and a pH value of 2.5 for 20min by using EM1713S regulated direct power, and the magnetic stirring speed was maintained at 400r/min. After electroplating, the plated cathode was cleaned with deionized water and then dried. The Ni-Co alloy porous electrodes prepared in the 0g/L WC and 30g/L WC solution were named $(Ni\text{-}Co)_0$ and $(Ni\text{-}Co)_{30}$, respectively.

2.2. Characterization and electrocatalytic HER performance test

The surface topography of $(Ni\text{-}Co)_0$ and $(Ni\text{-}Co)_{30}$ was tested by applying the HITACHI TM3030 scanning electron microscope (SEM). Their structural properties were analyzed by using an X-ray diffractometer (XRD) with the model of MINI FLEX 600 applying CuK_α radiation of wave length λ=0.154nm at tube voltage of 40kv and tube current of 15mA. The scanning rate of XRD is 0.02°/s and the scanning range is from 10° to 90°. CHI660E electrochemical workstation was used for electrocatalytic HER tests. All the electrochemical experiments were carried out in a three electrode chamber glass electrolyzer. The prepared $(Ni\text{-}Co)_0$ and $(Ni\text{-}Co)_{30}$ porous deposits were used as the working electrodes with a working area of 0.6cm^2. A large area Pt sheet was used as the counter electrode, and a saturated calomel electrode (SCE) acted as the reference electrode. While a solid salt bridge of agar-KCl with Luggin capillary was applyed to decrease the liquid junction potential between saturated KCl solution and the tested electrolyte, and reduce the iR drop caused by the solution resistance. The solution used for the electrocatalytic HER experiment was a 0.5M H_2SO_4 solution. The cathode linear scanning rate was 1mV/s, the cyclic voltammetry（CV）scanning rate was 20mV/s, and the sweep segments of CV was 20. The AC impedance of hydrogen evolution reaction were carried out in the frequency of 100kHz to 0.1Hz. The potential at -0.4V and -0.5V were taken as the initial potentials, respectively. The amplitude of the potential was kept at 5mV. At the potential of -0.5V, the amperometric i-t curves of HER were tested for 10h. The measurement of cathodic polarization curves of HER were carried out at various temperatures of 25℃ to 50℃, any other tests were controlled at temperature of 25℃ by using the HH-1 digital constant temperature water bath.

3. RESULTS AND DISCUSSION

The SEM images of $(Ni\text{-}Co)_0$ and $(Ni\text{-}Co)_{30}$, magnified 500, 5.0K and 10K times, are displayed in Fig.1, respectively. It can be found from the 500 times SEM morphologies in Fig.1(a) and Fig.1(d) that $(Ni\text{-}Co)_0$ and $(Ni\text{-}Co)_{30}$ electrodes have a 3-dimension cross-linked netlike structure. The surface of the porous skeleton of the $(Ni\text{-}Co)_0$ is relatively smooth, while a large number of particles are embedded in the mesh frame of the $(Ni\text{-}Co)_{30}$. The 5.0K× and 10K× SEM images displayed in Fig.1(b) and Fig.1(c)

show that the surface of the $(Ni\text{-}Co)_0$ deposit is relatively flat, which is evenly filled with a large number of dense fine particles.

It can be seen from the 5.0K× SEM image Fig.1(e) and 10K× SEM image Fig.1(f) that a large number of dense and strongly linked coarse particles with the shape of a peanut shell are distributed on the surface of $(Ni\text{-}Co)_{30}$ deposit. These large particles are actually composed of many tiny grains with a grain size of about 0.2 ~ 0.5μm.

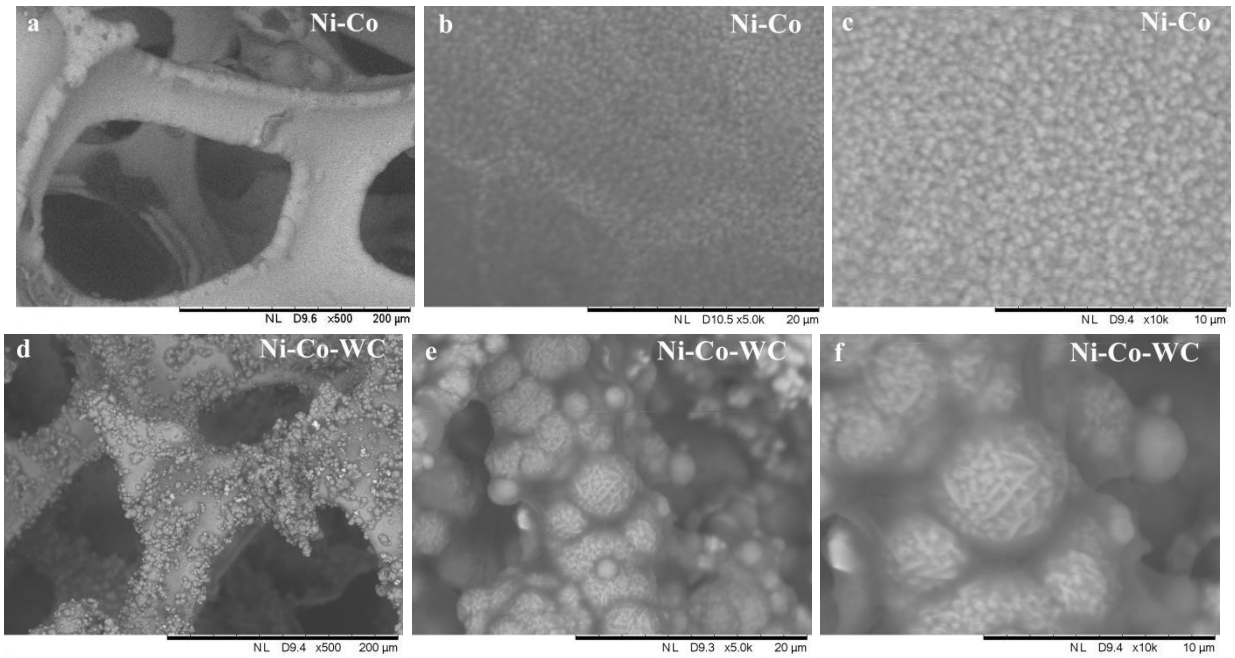

Figure 1. SEM images of $(Ni\text{-}Co)_0$ and $(Ni\text{-}Co)_{30}$ (a,b,c- $(Ni\text{-}Co)_0$, d,e,f- $(Ni\text{-}Co)_{30}$).

This is a special morphology formed by composite plating with WC particles during Ni-Co codeposition. Obviously, the $(Ni\text{-}Co)_{30}$ deposit is coarser with a higher specific surface area than that of the $(Ni\text{-}Co)_0$ deposit. Such a interconnected three-dimensional porous structure in $(Ni\text{-}Co)_0$ and $(Ni\text{-}Co)_{30}$ electrodes helps to provide larger and smoother channels for the sufficient contact between the H_2SO_4 solution and the HER electrode, which helps to increase the efficiency and the rate of mass transfer. Moreover, this interconnected electron transfer skeleton provides a large number of electrocatalytic HER active sites for the electrode, and provides an effective place for the generation, adsorption and desorption of active hydrogen atoms. Thus, it is beneficial to reduce the overpotential of HER and greatly improve the electrocatalytic HER activity of the electrode.

Fig.2 shows the XRD patterns of $(Ni\text{-}Co)_0$ and $(Ni\text{-}Co)_{30}$. $(Ni\text{-}Co)_0$ has a face centered cubic (FCC) crystal structure of Ni-Co alloy solid solution with Ni as the solvent. It can be seen from the XRD spectra of $(Ni\text{-}Co)_0$ that there are three diffraction peaks of Ni at 2θ angles of near 44.52°, 51.8° and 76.38°, which are (111), (200) and (220) planes, respectively. However, there are no diffraction peaks of Co phase, which attributes to the crystal lattice of Ni is partly replaced by Co and a Ni-Co solid solution is formed as a result of nucleation and growth mechanism [35]. The XRD pattern of $(Ni\text{-}Co)_{30}$ shows that (111) and (200) diffraction peaks of Ni appear at the same position, and the height of these

two peaks is greatly reduced, while the original (220) peak near 76.38° is divided into two small peaks, which may be due to the addition of WC in Ni-Co deposit. In addition, there are seven WC diffraction peaks at 2θ of 31.6°, 35.72°, 48.36°, 64.11°, 66°, 73.32° and 84.19°, which are (001), (100), (101), (110), (002) (111) and (201) planes respectively. Among them, there are two relatively sharp peaks, which are peak (100) and peak (101), respectively. XRD shows that $(Ni\text{-}Co)_{30}$ is a biphasic crystal structure composed of WC and Ni-Co alloy solid solution, with the second phase WC tiny particles dispersing in the Ni-Co deposit.

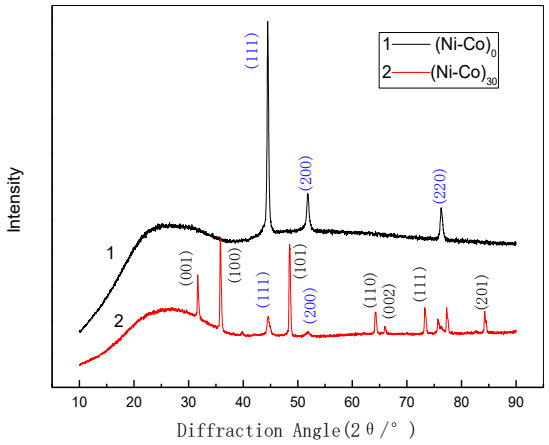

Figure 2. XRD patterns of $(Ni\text{-}Co)_0$ and $(Ni\text{-}Co)_{30}$.

When the temperature is 25℃, 30℃, 40℃ and 50℃, the HER polarization curves of porous $(Ni\text{-}Co)_0$ and porous $(Ni\text{-}Co)_{30}$ in 0.5M H_2SO_4 solution are shown in Fig.3.

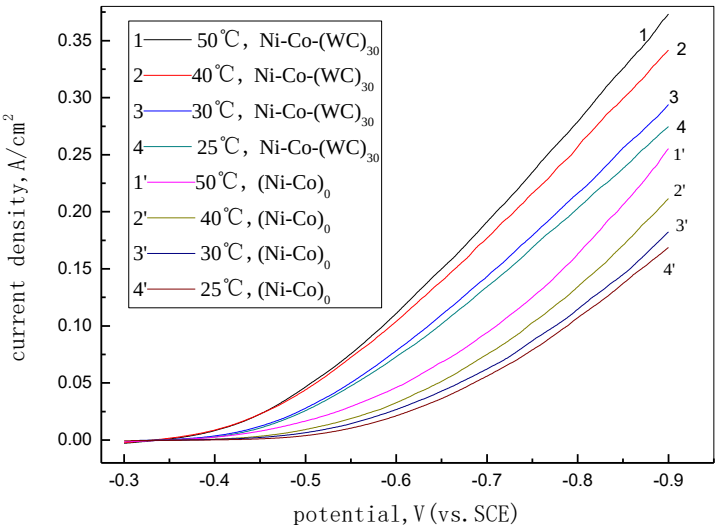

Figure 3. HER polarization curves of $(Ni\text{-}Co)_0$ and $(Ni\text{-}Co)_{30}$ in 0.5M H_2SO_4 (scan rate 1mV/s).

It was reported that apart from Pt, Rh, Pd and other noble metals, Ni showed the best HER activity among the transition metal[36]. Moreover, due to the synergistic effect, the hydrogen evolution activity of Ni-Co alloy is better than that of nickel. Fig.3 demonstrates that the HER onset potential of $(Ni\text{-}Co)_0$ and $(Ni\text{-}Co)_{30}$ is about -0.3V, which is lower than that of Pt NFC (-0.245Vvs.NHE, ca. -0.486Vvs.SCE)[37]. With the increase of solution temperature, the cathodic polarization curves of $(Ni\text{-}Co)_0$ (curves 1'-4') and $(Ni\text{-}Co)_{30}$ electrodes (curves 1-4) move towards positive potential, and their rate of HER improves with the rise of temperature. At the same time, the polarization curves of $(Ni\text{-}Co)_{30}$ is located in the more positive potential direction of $(Ni\text{-}Co)_0$, and its HER polarization resistance is much smaller than that of porous $(Ni\text{-}Co)_0$ electrode. At the same conditions of temperature and potential, the HER current density of $(Ni\text{-}Co)_{30}$ is larger and the HER rate is faster. When the temperature is 25℃, the relationship between HER overpotential η (V) and current density i (mA/cm^2) of $(Ni\text{-}Co)_0$ and $(Ni\text{-}Co)_{30}$ is shown in Fig.4. When the HER current densities are $10mA/cm^2$, $15mA/cm^2$, $20mA/cm^2$, $25mA/cm^2$ and $30mA/cm^2$, the HER overpotential of $(Ni\text{-}Co)_{30}$ is 0.118V, 0.123V, 0.129V, 0.133V and 0.137V lower than that of $(Ni\text{-}Co)_0$, respectively. The results show that when the reaction rate of HER is the same, the HER overpotential of $(Ni\text{-}Co)_{30}$ is smaller, the electrocatalytic HER performance of $(Ni\text{-}Co)_{30}$ is obviously more excellent than that of $(Ni\text{-}Co)_0$ electrode.

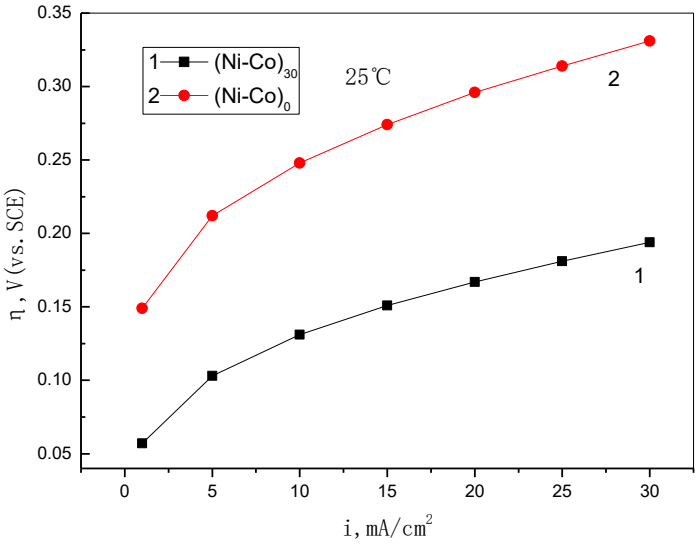

Figure 4. Relationship between HER overpotential and current density of $(Ni\text{-}Co)_0$ and $(Ni\text{-}Co)_{30}$ at 25℃.

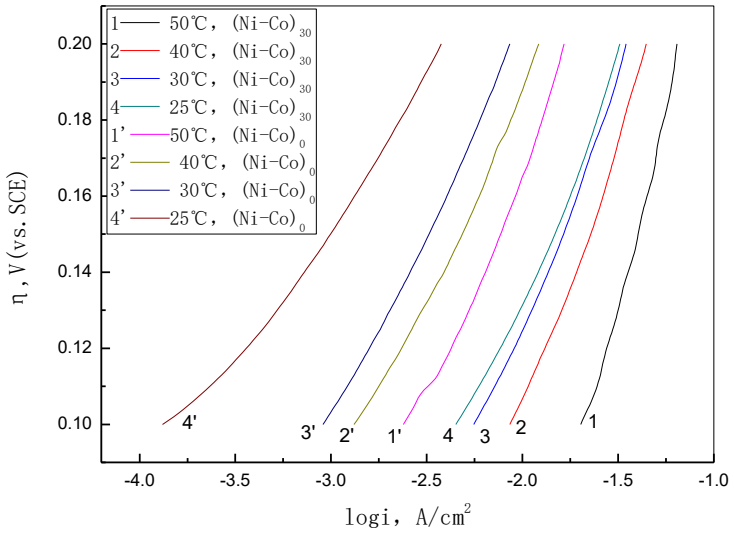

Figure 5. Tafel curves of $(Ni\text{-}Co)_0$ and $(Ni\text{-}Co)_{30}$ in 0.5M H_2SO_4 (scan rate 1mV/s).

Within a certain potential range with the overpotential greater than 100mV, the HER overpotential (η) of $(Ni\text{-}Co)_0$ (curves 1'-4') and $(Ni\text{-}Co)_{30}$ (curves 1-4) is almost linearly related to the logarithm of the current density (lg*i*), as shown in Fig.5. The intercept and slope of linear regression of each curves in Fig.5 and the kinetic parameters calculated by Tafel equation ($\eta=a+b\lg i$) are shown in Table1. Where, η (V) is the overpotential, a (V) is the intercept, b ($Vdec^{-1}$) is the slope, i_0 (mA/cm^2) is the apparent exchange current density, α is the electron exchange coefficient.

Table 1. Kinetic parameters of HER of $(Ni\text{-}Co)_0$ and $(Ni\text{-}Co)_{30}$ in 0.5M H_2SO_4 solution at various temperature

	$(Ni\text{-}Co)_0$				$(Ni\text{-}Co)_{30}$			
t, ℃	a, V	b, $Vdec^{-1}$	i_0, mA/cm^2	α	a, V	b, $Vdec^{-1}$	i_0, mA/cm^2	α
25	0.368	0.072	0.008	0.411	0.367	0.117	0.730	0.253
30	0.408	0.103	0.109	0.292	0.378	0.126	1.000	0.239
40	0.394	0.104	0.163	0.299	0.387	0.142	1.882	0.219
50	0.408	0.121	0.425	0.265	0.433	0.201	7.011	0.160

It can be seen from Tab.1 that the HER apparent exchange current density i_0 of $(Ni\text{-}Co)_0$ and $(Ni\text{-}Co)_{30}$ rises when the temperature increases. At the same temperature, the i_0 of $(Ni\text{-}Co)_{30}$ is far higher than that of $(Ni\text{-}Co)_0$. When the temperature is 25℃, 30℃, 40℃ and 50℃, the i_0 of $(Ni\text{-}Co)_{30}$ is 90.25, 8.174, 10.546 and 15.496 times greater than that of the $(Ni\text{-}Co)_0$, respectively. It shows that the addition of WC in Ni-Co deposit by composite plating is conducive to improve the HER rate of Ni-Co and greatly enhance its electrocatalytic HER activity. Tab.2 also shows that the $(Ni\text{-}Co)_{30}$ electrode has better HER activity than some other reported electrocatalysts.

Table 2. Comparison of i_0 of the $(Ni\text{-}Co)_{30}$ and other catalysts

Catalysts	i_0, mA/cm^2	T,℃	Electrolyte	References
$(Ni\text{-}Co)_{30}$	0.730	25	0.5M H_2SO_4	This work
$(Ni\text{-}Co)_{30}$	1.000	30	0.5M H_2SO_4	This work
NiMo	0.158	room temperature	0.78M H_2SO_4	[38]
rhenium oxides	0.0027	25	0.5M H_2SO_4	[39]
Pt/C	0.32	room temperature	0.5M H_2SO_4	[40]
Ni-2.26wt % CeO_2 Gd	0.1231	room temperature	0.5M H_2SO_4	[41]
Pd	0.91	25	0.5M H_2SO_4	[42]

When the initial potentials are kept at -0.4V and -0.5V respectively, the EIS for HER of $(Ni\text{-}Co)_0$ and $(Ni\text{-}Co)_{30}$ porous electrodes in 0.5M H_2SO_4 solution at 25°C is shown in Fig.6. The EIS shows that the solution resistance is very small, and there is no slash with an angle of 45° in the AC impedance spectra of the two electrodes in the low frequency region, which indicates that no obvious concentration polarization occurs during the HER [43]. The EIS for HER of both $(Ni\text{-}Co)_0$ and $(Ni\text{-}Co)_{30}$ are two semicircular arcs of various diameters located in the first quadrant, indicating that the mechanism of HER of the two electrodes is the same. Moreover, the rate of HER of $(Ni\text{-}Co)_0$ and $(Ni\text{-}Co)_{30}$ is significantly influenced by their surface state.

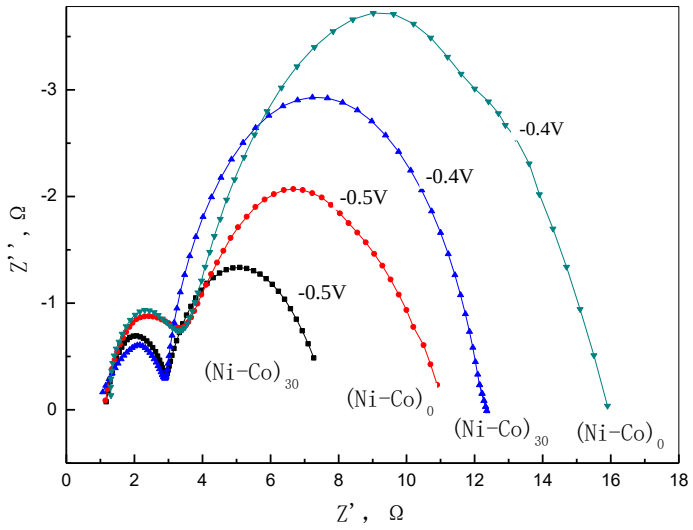

Figure 6. EIS of $(Ni\text{-}Co)_0$ and $(Ni\text{-}Co)_{30}$ in 0.5M H_2SO_4 solution at 25°C and different potentials.

When the initial potential shifts from -0.4V to -0.5V, the two semi-circle diameters of the EIS of $(Ni\text{-}Co)_0$ and $(Ni\text{-}Co)_{30}$ decreases, indicating that their HER resistance decreases. In other words, as the initial potential moves towards the negative potential, the HER rate of $(Ni\text{-}Co)_0$ and $(Ni\text{-}Co)_{30}$ is accelerated.

The mechanism of HER in acidic solution includes the formation of adsorbed H intermediate M-H_{ads}, electrochemical desorption reaction and chemical desorption process [24,44-48], which corresponds to the Volmer reaction, Heyrovsky reaction and Tafel process, respectively. Namely:

$M + H^+ + e^- \rightarrow M\text{-}H_{ads}$ (Volmer reaction)

$M\text{-}H_{ads} + H^+ + e^- \rightarrow H_2 + M$ (Heyrovsky reaction)

$M\text{-}H_{ads} + M\text{-}H_{ads} \rightarrow H_2 + 2M$ (Tafel reaction)

The Tafel slope value can imply the mechanism of hydrogen reduction on cathodes [49]. In acidic soluiton, the theoretical HER Tafel slopes for the Volmer step, Heyrovsky step, and Tafel step are 120, 40, and 30mVdec-1, respectively [50-52]. The Tafel slope of $72mVdec^{-1}$ and $117mVdec^{-1}$ for $(Ni\text{-}Co)_0$ and $(Ni\text{-}Co)_{30}$, respectively, which is between 40-120$mVdec^{-1}$, indicates that HER occurred via a Volmer- Heyrovsky step. Fig. 6 shows that the diameter of the second arc of the EIS of both $(Ni\text{-}Co)_0$ and $(Ni\text{-}Co)_{30}$ is much larger than that of the first arc, indicating that the adsorbent resistance in the form of capacitance is greater than the electrochemical reaction resistance. The two semicircular arcs in the first quadrant show that the change of coverage of adsorbed H_{ads} on the surface of $(Ni\text{-}Co)_0$ and $(Ni\text{-}Co)_{30}$ has a greater influence on the Heyrovsky reaction than on the Volmer reaction. Fig.7 shows the corresponding fitting equivalent circuit diagram (FECD). The constant phase angle element (CPAE) equation is:

$$Z = R_1 + \frac{R_2 + R_3 + j\omega R_2 R_3 C_2}{1 + j\omega R_3 C_2 + (j\omega)^2 R_2 R_3 C_2 C_1}$$

Where, R_1 is the ohmic resistance of the electrolyte, R_2 is the charge-transfer resistance of HER, R_3 is the adsorbent resistance of H_{ads}, C_1 and C_2 is the double-layer capacitance and the adsorbent capacitance, respectively.

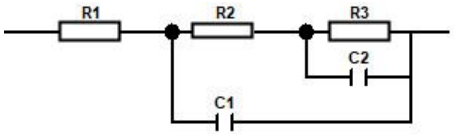

Figure 7. FECD for the HER on $(Ni\text{-}Co)_0$ and $(Ni\text{-}Co)_{30}$ in 0.5M H_2SO_4 solution at 25°C.

The fitting parameters for EIS in Fig. 6 are listed in Table 3. At the same potential, the charge transfer resistance R_2 of $(Ni\text{-}Co)_{30}$ is lower than that of $(Ni\text{-}Co)_0$. Similarly, the adsorbent resistance R_3 of $(Ni\text{-}Co)_{30}$ is smaller than that of $(Ni\text{-}Co)_0$. The decrease of resistance further shows that $(Ni\text{-}Co)_{30}$ has better activity of electrocatalytic HER than that of $(Ni\text{-}Co)_0$.

Table 3. Fitting parameters for EIS of $(Ni\text{-}Co)_0$ and $(Ni\text{-}Co)_{30}$ in 0.5M H_2SO_4 solution at 25℃ and at potential of -0.4V and -0.5V

electrode	$(Ni\text{-}Co)_0$		$(Ni\text{-}Co)_{30}$	
Potential, V(vs.SCE)	-0.4	-0.5	-0.4	-0.5
R_1, Ω	1.297	1.302	1.293	1.287
R_2, Ω	2.043	1.982	1.462	1.546
R_3, Ω	8.417	5.210	6.193	3.212
C_1, Fcm^{-2}	1.892×10^{-5}	1.791×10^{-5}	1.897×10^{-5}	1.917×10^{-5}
C_2, Fcm^{-2}	1.601×10^{-3}	1.284×10^{-3}	4.987×10^{-3}	5.033×10^{-3}

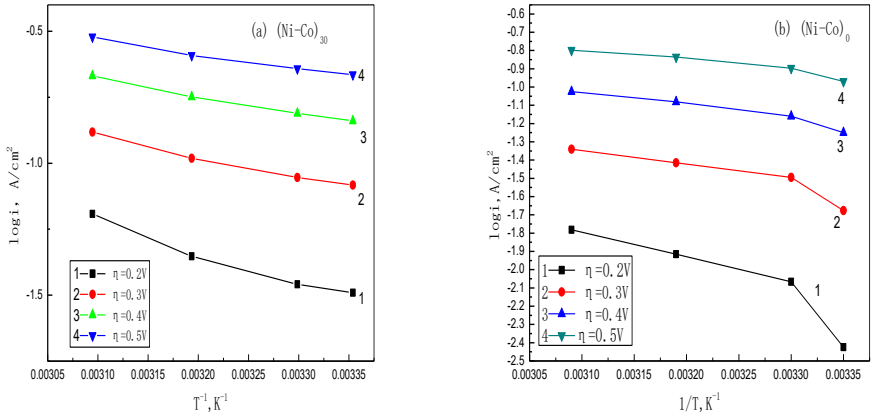

Figure 8. 1/T~ logi curves of $(Ni\text{-}Co)_0$ and $(Ni\text{-}Co)_{30}$ at various η.

The 1/T~log*i* relationship curves of $(Ni\text{-}Co)_{30}$ and $(Ni\text{-}Co)_0$ at the overpotential (η) of 0.2V, 0.3V, 0.4V and 0.5V are obtained from Fig.3 and shown in Fig.8(a) and Fig. 8(b), respectively. The curves in Fig.8 are almost linear. The apparent activation energy E(η) of HER of $(Ni\text{-}Co)_0$ and $(Ni\text{-}Co)_{30}$ at the above overpotential is derived from the fitted slope of each curve in Fig.8, as shown in Table 4.

Table 4. slope and E(η) of $(Ni\text{-}Co)_0$ and $(Ni\text{-}Co)_{30}$ in 0.5M H_2SO_4 solution at various η

	$(Ni\text{-}Co)_{30}$ electrode		$(Ni\text{-}Co)_0$ electrode	
η,V(vs.SCE)	Slope, K	E(η), kJ/mol	slope	E(η), kJ/mol
0.2	-1154	22	-2198	42
0.3	-774	15	-1158	22
0.4	-654	13	-820	16
0.5	-549	11	-621	12

Tab.4 shows that the apparent HER activation energy of $(Ni\text{-}Co)_0$ and $(Ni\text{-}Co)_{30}$ porous electrodes reduces with increasing cathodic overpotential. At the same overpotential, the apparent activation energy of HER of $(Ni\text{-}Co)_{30}$ is less than that of $(Ni\text{-}Co)_0$. The results show that $(Ni\text{-}Co)_{30}$ has better

electrocatalytic HER activity. This may be due to addition the tiny particles of WC in the deposit, which makes $(Ni\text{-}Co)_{30}$ has larger specific surface area and higher surface roughness than $(Ni\text{-}Co)_0$, which can further reduce the HER overpotential and improve its activity of electrocatalytic HER.

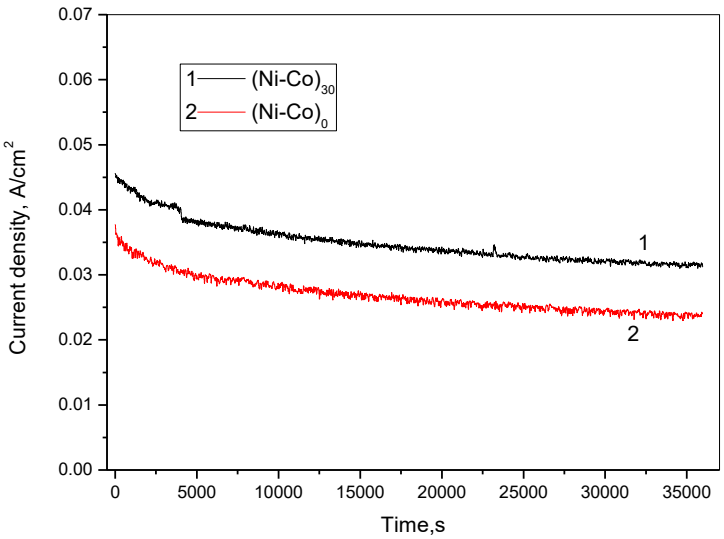

Figure 9. i-t curves of $(Ni\text{-}Co)_0$ and $(Ni\text{-}Co)_{30}$ at 25°C and in 0.5M H_2SO_4 solution.

The HER stability of the electrodes was studied by chronoamperometry and cyclic voltammetry (CV). As the potential and time are kept at -0.5V（η=0.2V）and 10h respectively, the chronoamperometry curves of $(Ni\text{-}Co)_0$ and $(Ni\text{-}Co)_{30}$ porous electrodes for potentiostatic electroanalysis of HER at 25°C and in 0.5M H_2SO_4 solution are shown in Fig.9.

In the whole electrolysis process, the i-t curves of $(Ni\text{-}Co)_{30}$ and $(Ni\text{-}Co)_0$ have similar change rules. At the initial time, their HER current density is 45.62mA/cm^2 and 37.77mA/cm^2, respectively, then the curves gradually decrease in the first 4000s, and the current density basically tends to keep the stable value of 38mA/cm^2 and 30mA/cm^2 in a short time, which is a process from unsteady state to quasi steady state. This may be caused by the gradual consumption of reactants on the electrode surface and the gradual increase of the thickness of the diffusion layer. It is reported that the HER current density of electrocatalysts Pt/C and Pd/C in 0.5M H_2SO_4 solution decreased drastically for 6h, and then tends to stabilize [53]. The initial unstable transition time of Pt/C and Pd/C is much longer than that of $(Ni\text{-}Co)_{30}$ and $(Ni\text{-}Co)_0$. Obviously, the stability of HER of $(Ni\text{-}Co)_{30}$ and $(Ni\text{-}Co)_0$ is better than that of Pt/C and Pd/C. Over time, the i-t curves become relatively flat and the current density does not change dramatically, indicating that the electrocatalytic HER performance of $(Ni\text{-}Co)_{30}$ and $(Ni\text{-}Co)_0$ does not decay significantly, the HER stability of the two electrodes is good. It can be found from Fig.9 that the HER current density of $(Ni\text{-}Co)_{30}$ is greater than that of $(Ni\text{-}Co)_0$, which further shows that the HER property of $(Ni\text{-}Co)_{30}$ is superior to $(Ni\text{-}Co)_0$. After electrolysis for 10h, the minimum HER current density of $(Ni\text{-}Co)_{30}$ and $(Ni\text{-}Co)_0$ in the i-t curves is still as high as about 31.09mA/cm^2 and

22.93mA/cm^2, respectively. Fig.10 shows the CV curves of the $(Ni\text{-}Co)_{30}$ and the $(Ni\text{-}Co)_0$ in 0.5M H_2SO_4 solution at 25℃ with 10 cycles. Obviously, the CV curve of $(Ni\text{-}Co)_{30}$ is located in the positive potential direction of $(Ni\text{-}Co)_0$, and the two curves are far apart, showing that the HER current density of $(Ni\text{-}Co)_{30}$ is much higher than that of $(Ni\text{-}Co)_0$. It is also found that there are no anodic oxidation peaks on the anode reverse scanning direction, indicating that the corrosion resistance of the two electrocatalytic HER materials in the diluted sulfuric acidic solution is good, or their dissolution is negligible.

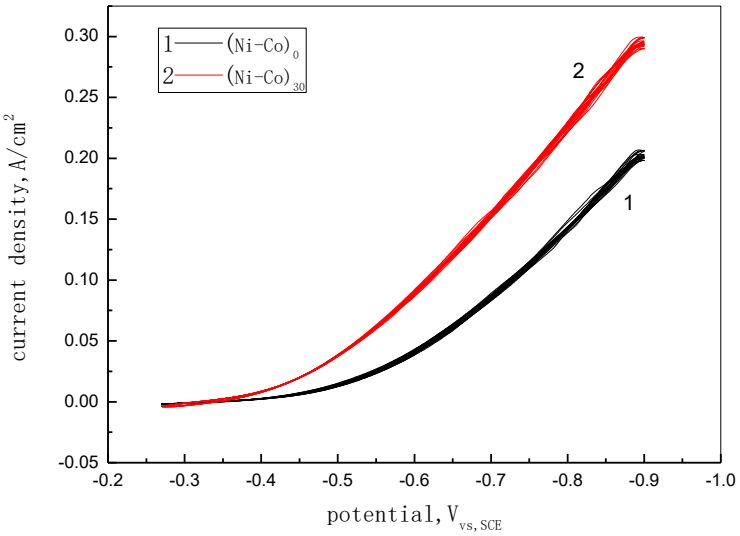

Figure 10. CV curves of $(Ni\text{-}Co)_0$ and $(Ni\text{-}Co)_{30}$ in 0.5M H_2SO_4 solution at 25℃ (sacn rate 10mV/s)

According to Fig.10, when the potential is kept at -0.4V and -0.45V respectively, the relationship between the HER current density of the two electrodes and cycle times is shown in Fig.11. In the whole cyclic voltammetry process, with the increase of recycle times, the HER current density of $(Ni\text{-}Co)_{30}$ and $(Ni\text{-}Co)_0$ at the same potential has no obvious attenuation, indicating that both electrodes have good HER stability.

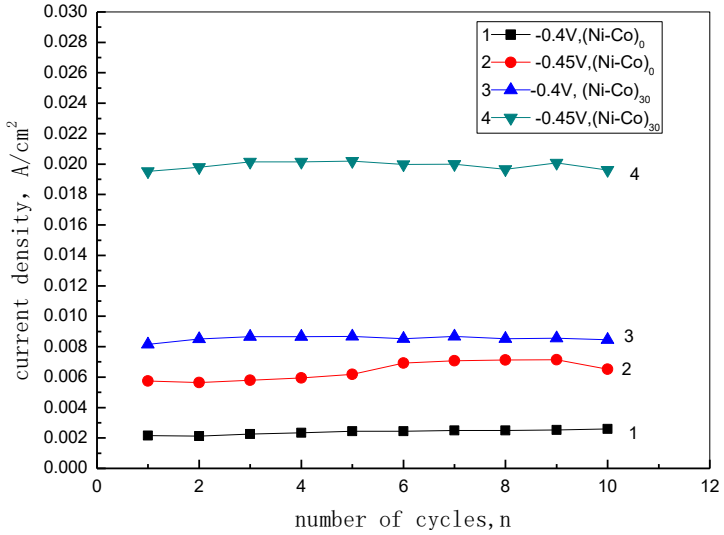

Figure 11. Relationship curve between cycle times and current density of $(Ni\text{-}Co)_0$ and $(Ni\text{-}Co)_{30}$ in 0.5M H_2SO_4 solution.

4. CONCLUSIONS

$(Ni\text{-}Co)_0$ and $(Ni\text{-}Co)_{30}$ porous electrodes were manufactured by electroplating on a Co based alloy $Co_{69.9}Ni_{30.1}$ foam substrate. Their HER properties in 0.5M dilute sulfuric acid solution were tested. Comparing with the porous $(Ni\text{-}Co)_0$, the porous $(Ni\text{-}Co)_{30}$ has smaller cathodic polarization and AC impedance, lower HER activation energy and larger HER exchange current density. At the same temperature, the HER exchange current density of $(Ni\text{-}Co)_{30}$ is much higher than that of $(Ni\text{-}Co)_0$, showing excellent electrocatalytic HER activity. Like the $(Ni\text{-}Co)_0$, the $(Ni\text{-}Co)_{30}$ is not easy to be oxidized. It exhibits higher HER stability in the 10h potentiostatic electrolysis HER test with a much higher HER current density than that of $(Ni\text{-}Co)_0$.

ACKNOWLEDGMENTS
This work was supported by the Innovative Project of Guangdong Education Department (Grant No. 2016KTSCX084).

References

1. I. Dincer, *Int. J. Hydrogen Energy*, 27 (3) (2002) 265.□
2. S. Dunns, *Int. J. Hydrogen Energy*, 27 (3) (2002) 235.□
3. F. Barir, *Sol. Energy*, 78 (5) (2005) 661.
4. H. Lund, *Energy*, 32 (6) (2007) 912.
5. C. J. Winter, *Int. J. Hydrogen Energy*, 34 (14-Sup1) (2009), S1.
6. C. Deng, X. Duan, J. Zhou, X. Zhou, W. Yuan, S. L. Scott, *Catal Sci. Technol.*, 5 (2015) 1540.

7. H. Yu, S. Cao, B. Fu, Z. Wu, J. Liu, L. Piao, *Catal. Commun*., 127 (2019) 1.
8. Jovic V. D., *Zastita Mater*., 52(2) (2011) 95.
9. T. C. Yuan, R. D. Li, H. J. Liu, K. C. Zhou, *J. Funct. Mater*., 40 (7) (2009) 1121.
10. Z. Zhang, L. Cong, Z. Yu, L. Qu, W. Huang, Mater., *Today Energy*, 16 (2020) 100387.
11. J. Yang, Z. D. Wu, *Chin. J. Rare Metals*, 22 (4) (1998) 251.
12. J. M. Jaksic, M. V. Vojnovic, N. V. Krstajic, *Electrochim. Acta*, 45 (2000) 4151.
13. J. Kubisztal, A. Budniok, A. Lasia, *Int. J. Hydrogen Energy*, 32 (2007) 1211.
14. N. V. Krstaji, V. D. Jovi, L. J. Gaji-Krstaji, B. M. Jovi, A. L. Antozzi, G. N. Martelli, *Int. J. Hydrogen Energy*, 33 (2008) 3676.
15. Q. Han, S. Cui, N. W. Pu, J. S. Chen, K. R. Liu, X. J. Wei, *Int. J. Hydrogen Energy*, 35 (2010) 5194.
16. H. X. Wei, Z. F. Zhou, D. F. Lv, Q. Ma, *Ship Science and Technology*, 33 (9) (2011) 124.
17. G. Tian, S. Wu, Z. Chen, Y. Cao, J. Tu, X. Tian, W. Huang, J. Wang, L. Ding, *Catal. Commun*., 159 (2021) 106350.
18. C. Lupi, A. Dell'Era, M. Pasquali, *Int. J. Hydrogen Energy*, 34 (2009) 2101.
19. González-Buch, I. Herraiz-Cardona, E. Ortega, J. García-Antón, V. Pérez-Herranz, *Int. J. Hydrogen Energy*, 38 (25) (2013) 10157.
20. C. Lupi, A. Dell' Era, Pasquali, *Int. J. Hydrogen Energy*, 39 (2014) 1932.
21. T. T. Sun, J. Cao, J. Dong, H. Y. Du, H. J. Zhang, J. F. Chen, L. B. Xu, *Int. J. Hydrogen Energy*, 42 (10) (2017) 6637.
22. S. H. Hong, S. H. Ahn, J. Choi, J. Y. Kim, H. Y. Kim, H. J. Kim, J. H. Jang, H. Kim, S. K. Kim, *Appl. Surf. Sci.*, 49 (2015) 629.
23. F. Rosalbino, S. Delsante, G. Borzone, E. Angelini, *J. Alloys Compd*., 429 (1-2) (2007) 270.
24. J. Vijayakumar, S. Mohan, S. Anand Kumar, S. R. Suseendiran, S. Pavithra, *Int. J. Hydrogen Energy*, 38 (25) (2013) 10208.
25. Subramanya, Y. Ullal, S. U. Shenoy, D. K. Bhat, A. C. Hegde, *RSC Advances*, 5 (59) (2015) 47398.
26. C. Fan, D. L. Piron, P. Paridis, *Electrochim. Acta*, 39 (1994) 2715.
27. D. Gao, J. N. Guo, X. Cui, L. Yang, Y. Yang, H. C. He, P. Xiao, Y. H. Zhang, *ACS Appl Mater Interfaces*, 9 (2017) 22420.
28. P. R. Zabinski, S. Meguro, K. Asami, K. Hashimoto, *Mater. Trans.*, 47 (2006) 2860.
29. S. L. Wang, Q. H. Duan, *T. Nonferr. Metal Soc*., 23 (8) (2013) 2221.
30. Q. H. Duan, S. L. Wang, L. P. Wang, *Acta Phys. Chim. Sin*., 29 (1) (2013) 123.
31. J. G. Zhang, S. M. Zhang, C. F. Li, L. M. Wang, S. Li, D. R. Meng, *Chinese Journal of Rare Metals*, 42 (7) (2018) 673.
32. Q. Zhou, D. K. Ouyang, F. Wang, J. S. He, X. B. Li, *Chin. J. Inorg. Chem*., 37 (3) (2021) 412.
33. H. Liu, J. N. Liu, Z. Q. Xu, W. Y. Zhou, C. Han, G. C. Yang, Y. P. Shan, Appl. Su*rf. Sci*., 572 (000) (2022) 151482.
34. Y. F. Yang, X. Zhu, B. D. Zhang, H. Yang, C. J. Liang, *Int. J. Hydrogen Energy*, 44 (2019) 19771.
35. Tury B., Lakatos-Varsanyi M., Roy S., *Surf. Coat. Tech.* 200 (2006) 6713.
36. A. B. Laursen, A. S. Varela, F. Dionigi, H. Fanchiu, C. Miller, O. L. Trinhammer, J. Rossmeisl, S. Dahl, *J. Chem. Educ*. 89 (2012) 1595.
37. B. Rezaei, M. Mokhtarianpour, A. A. Ensafi, *Int. J. Hydrogen Energy*, 40 (2015) 6754.
38. Savidra Lucatero, Gabriel Tamayo, Diego Crespo, Ernesto Mariño and Marcelo Videa, *J. New Mat. Electr. SysS*., 16 (2013) 177.
39. Alejandro Vargas-Uscategui, Edgar Mosquera, Boris Chornik, Luis Cifuentes, *Electrochimica Acta*, 178 (2015) 739.
40. Y. Zhang, Y. H. Wang, S. P. Jia, H. Q. Xu, J. B. Zang, J. Lu, X. P. Xu, *Int. J. Hydrogen Energy*, 42 (2017) 4741.
41. P. Sivasakthi, S. Premlatha, G.N.K. Ramesh Bapu, Maruthai Chandrasekaran, *Int. J. Hydrogen*

Energy, 42 (2017) 4741.
42. B. M. Jovic, V. D. Jovic, G. Brankovic, M. Radovic, N. V. Krstajic, *Electrochimica Acta*, 224 (2017) 571.
43. Y. F. Yang , H. Yang, C. J. Liang, X. Zhu, *Int. J. Electrochem. Sci.,* 13 (2018) 7193.
44. W. A. Badawy, H. Nady, M. Negem, *Int. J. Hydrogen Energy*, 39 (2014) 10824.
45. D. Gao, J. N. Guo, X. Cui, L. Yang, Y. Yang, H. C. He, P. Xiao, Y. H. Zhang, *ACS Appl. Mater. Interfaces*, 9 (2017) 22420.
46. A. Lasia, A. Rami, *J. Electroanal. Chem*., 294 (1990) 123.
47. Y. Li, H. Wang, L. Xie, Y. Liang, G. Hong, H. Dai, *J. Am. Chem. Soc*. 133 (2011) 7296.
48. M. Zeng, Y. Li, *J. Mater. Chem. A.* 3 (2015) 14942.
49. Y. Li, H. Wang, L. Xie, Y. Liang, G. Hong, H. Dai, *J. Am. Chem. Soc*., 133 (2011) 7296.
50. Z. Pu, Q. Liu, A.M. Asiri, A.Y. Obaid, X. Sun, *J. Power Sources*, 263 (2014) 181.
51. X. Zhao, H. Zhua, X. Yang, *Nanoscale,* 6 (2014) 10680.
52. Y. Li , P. Yang , B. Wang, Z. Q. Liu, *Journal of Nanotechnology*, 10 (2019) 62.
53. Y. H. Huang, K. D. Seo, D. S. Park, H. Park, Y. B. Shim, *Small*, 17(2021) 2007511.